



OPEN Failure and development height of overlying rock of a water flowing fracture in goaf under a karst aquifer

Lulin Zheng^{1,3✉}, Xiong Liu¹, Qing Qiu¹, Youwen Tian², Weide Ren², Jin Xu¹ & Xiaokun Wang¹

The factors leading to mine water inrush accidents are mainly sources of water, water channels, and intensity of water inrush. Mine water rush depends mostly on whether damage leads to the overlying strata of the working face penetrating the overlying aquifer. There is therefore a need to characterize how the overlying strata of the coal seam roof fails and the development height of the water-conducting fracture zone during a roof water inrush incident. This study focuses on the Longfeng Coal Mine, northern Guizhou coalfield. Samples of rock from the roof coal seam were obtained by drilling and coring and examined under a scanning electron microscope. The results showed an undeveloped state of primary cracks in the overlying strata of the coal seam roof, with the water channel occurring mainly along mining-induced cracks. Four key strata were identified, and their fracture steps were calculated through integrating the results of the physical test of the overlying rock of the coal seam. The key strata break when the advancing distance of the working face exceeds their fracture steps. At this point, water-conducting cracks develop upwards. Simulation by FLAC3D allowed the analysis of vertical displacement, vertical stress, and evolution of the plastic zone of the roof overburden rock under different working face advancing distances. The results show that the changes in vertical stress and displacement in overburden rock initially increased rapidly, with this rate of increase subsequently slowing. The shape and maximum height of the plastic failure zone was typical trapezoid and 46.12 m, respectively. Finally, the height of the water-conducting fracture zone determined on site was 42–51.8 m. The good agreement between numerical simulation and measurements confirms that the results of this study can guide practical engineering.

Keywords Mine water inrush, Rule of overlying strata damage, Height of fractured water-conducting zone, Key stratum, FLAC3D

China has abundant coal resources and coal accounted for 55.3% of total national energy consumption in 2023. It is projected that coal will remain the main source of energy in China in the future¹. There were 1,465 coal mining-related accidents in China between 2008 and 2023, resulting in 5,473 deaths. Among them, there were 164 water-related accidents which resulted in 776 deaths, accounting for 11.2% of total accidents and 14.2% of total deaths, respectively². Mine water disasters can also result in major geological hazards, including declines in groundwater level and surface subsidence. These phenomena have a significant negative impact on surface infrastructure, agriculture, and the natural environment³. Guizhou is an important coal-producing area in China⁴ and is known as the “coal sea in the area south of the Yangtze River”. Guizhou falls within an area of typical high karst concentration exceeding 60%⁵. Underground rock shows well developed dissolution cracks, with many areas in a transitional state between developed karst and coal resources, with the northern Guizhou coalfield being a typical example. The northern Guizhou coalfield is the third largest in Guizhou and has experienced multi-stage tectonic movements, contributing to complex geological conditions. Since its minable coal seams mainly occurs in the Longtan Formation of the Upper Permian, it can be classified as marine-terrestrial sedimentary facies⁶. The coal mining face has for an extended period been affected by being positioned between the overlying Changxing Formation and the limestone karst water of the underlying Maokou Formation. While the mine receives ample water, the aquifuge between the coal mining face and the aquifer is thin. Mining can readily result

¹Mining College, Guizhou University, Guiyang 550025, China. ²Guizhou Lindong Coal Industry Development Co., Ltd. Longfeng Coal Mine, Jinsha Guizhou 551800, China. ³College of Resources and Environment, Guizhou University, Guiyang 550025, China. ✉email: llzheng@gzu.edu.cn

in the water-conducting fracture zone penetrating the overlying aquifer, causing water inrush accidents. The water inrush incident on 21st August, 2019 in the Longfeng Coal Mine, northern Guizhou coalfield, resulting in 2 deaths; a water and sand inrush incident on 19th June, 2022 at the Tenglong Coal Mine, adjacent to Longfeng Coal Mine, resulting in 1 death, 1 loss of contact, and 1 injury. These two incidents could be mainly attributed to a failure to fully understand the timescales over which mining influences the water-conducting fracture zone of the mine under complex geological conditions as well as the mechanisms of water inrush from the roof overburden rock.

There have been many studies, both in China and internationally, on failure of overlying strata of a coal seam roof and the development height of the water flowing fractured zone. Internationally, a Belgian study proposed the “vertical line theory” explaining overburden failure⁷; a study in France proposed the “arch theory” and “zoning theory”⁸ explaining overburden deformation and failure; a German study proposed the “cantilever beam theory” to explain periodic pressure⁹; another German study proposed the “pressure arch” hypothesis¹⁰; a Belgian study proposed the “pre-fracture hypothesis” explaining how the equilibrium of rock inside the overburden is disrupted after mining, leading to the formation of various fractures¹¹; a study in the former Soviet Union proposed the “hinged rock block” hypothesis, which places rock strata into three categories: the irregular caving, regular caving, and regular moving zones¹². Domestically, the “masonry beam” theory was proposed, explaining the formation of large and small structures¹³; the “transfer rock beam” hypothesis, suggested that strata sensitive to the distribution and manifestation of mining pressure comprises “immediate roof” and “main” roof layers, with the latter comprised of transfer rock beams. Fracturing results in the formation of internal and external stress fields in the surrounding coal seam. Spatial variation in the stress field in relation to the direction of the working face aligns with the fracturing direction of each rock beam in the main roof^{14–16}.

Previous Chinese studies applied traditional empirical simulation methods to characterize the height of the water-conducting fracture zone^{17,18}. These previous studies identified the cubic function polynomial curve as optimal for predicting the height of the water-conducting fracture zone of the coal seam roof for mechanized caving mines. There have also been many previous applications of numerical models to determine the height of water-conducting fracture zone. Currently, the commonly used numerical simulation software includes UDEC, FLAC3D, 3DEC, and PFC. Studies applying these models include integrating the shaking table test and FLAC3D numerical simulation to simulate the seismic response of the active ground fissure site and to analyze the dynamic characteristics of the ground fissure site¹⁹; the application of UDEC to simulate mining-induced uplift²⁰; the calculation of inter-block force based on the rigid body displacement constraint method of 3DEC platform and the creation of 3DEC-KBM to analyze the stability of fractured rock slopes and fractured rock masses around underground caverns²¹; the application of PFC3D to identify the relative influences of different fracture characteristics on rock strength and to identify the effect of dip angle on rock crack propagation²²; the application of FLAC3D to study the development and evolution of fractures and the three-dimensional distribution of water-conducting fracture zones, which led to the development of the elastic wave exploration method for predicting the height of water-conducting fracture zones²³.

While the above studies have contributed significantly to improved understanding of overburden failure and water-conducting fractures, further research is needed given the complex geological conditions of northern Guizhou coalfield. Using the 120,905 working face of Longfeng Coal Mine as a study area, the present study aimed to characterize failure roof overburden and the height of the water-conducting fracture zone. The results of the present study can contribute to the prevention and amelioration of water disasters in mines in northern Guizhou and those under similar hydrogeological conditions.

Materials

Engineering situations

Longfeng Coal Mine is located in the northern Guizhou Plateau, with a production scale of 900,000 tons/year. At present, the main mining 9# coal seam is fully mechanized and fully mechanized. The coal seam adopts the strike longwall mining method, one-time mining full height, retreating mining, and the roof is managed by the full caving method. The mining area is dominated by karst peak cluster landform. The karst development in the area is strong and uneven. The strata of the mining area from old to new are: Maokou Formation, Longtan Formation, Changxing Formation, Shabaowan Section of Yelang Formation, Yulongshan Section of Yelang Formation, and Jiujitan Section of Yelang Formation, as shown in Fig. 1. Among them, Yulongshan section, Changxing Formation and Maokou Formation are soluble rocks, with developed dissolution fissures and strong water richness. The surface faults in the area are not developed. Except that one fault running through the production roadway in the mining area has good water conductivity, the other faults do not conduct water and have little influence on coal mining. The strike of coal seam in the whole area is relatively gentle, and the average dip angle of coal seam is 7°, which belongs to the near horizontal coal seam. The roof lithology is mainly sandstone, mudstone and argillaceous siltstone. The roof of the coal seam is mostly less than 80 m from the bottom boundary of the limestone aquifer of the Changxing Formation. The mining fissure is easy to conduct the overlying Changxing Formation aquifer, which threatens the safety of the working face.

Analysis of roof overburden characteristics of working face

Analysis of microstructure characteristics of overlying strata rock

The macroscopic mechanical behavior of rock is usually controlled by its microstructure, and the deformation and failure of rock under load are affected by its microscopic morphological characteristics^{24–26}. In order to understand the microstructure of overlying strata of No.9 coal seam roof in Longfeng Coal Mine, the rock samples obtained by drilling coring were observed by electron microscope scanning technology, and the results were shown in Fig. 2. In the Fig. 2, the pink ellipse represents holes and pores, and the yellow ellipse range represents cracks. A and B are siltstones. The rock is dense, and micro-cracks are locally developed. The fracture

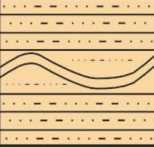
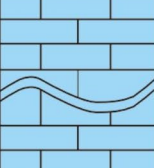

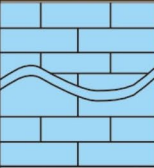

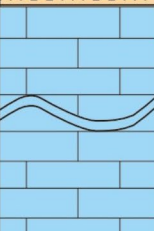
stratigraphic age					thickness (m)	histogram 1:200	Coal seam number	hydrogeological characteristics
system	series	group	segment	code				
Triassic	Lower Series	Yelang Group	Jiuji Bank section	T_1Y^3	164			The lithology is mainly thin to medium-thick silty mudstone and argillaceous siltstone. The thickness is 154-178 m, with an average thickness of 164 m. The underground runoff modulus is less than $1L/S \cdot km^2$. Water-rich is weak, for the relative aquiclude.
			Yulong Mountain section	T_1Y^2	208			The lithology is mainly thin to medium thick limestone, 194-216 m thick. The average thickness is 208 m. Karst cave water containing fissures, underground runoff modulus $1-6L/S \cdot km^2$. Water-rich medium to strong, medium to strong water layer.
			Shabao Bay section	T_1Y^1	16			The lithology is mainly thin mudstone and siltstone mudstone, with a thickness of 3-19 m. The average thickness is 16m. The underground runoff modulus is less than $1L/S \cdot km^2$. Water-rich is weak, for the relative aquiclude.
Permian	Upper Series	Changxing Group		P_3c	39			The lithology is mainly medium-thick to thick limestone, 32-53 m thick. The average thickness is 39m. Karst cave water containing fissures, underground runoff modulus $1-6L/S \cdot km^2$. Water-rich medium to strong, medium to strong water layer.
		Longtan Group		P_3l	98		4# 5# 9# 13#	The lithology is mainly thin to medium-thick sandstone, mudstone and siltstone. The coal bearing formation is 82-107 m thick, with an average thickness of 98 m. Mineable coal seam in the area It is 4 #, 5 #, 9 # and 13 #. The underground runoff modulus is less than $1L/S \cdot km^2$. Water-rich is weak, for the relative aquiclude.
	Middle Series	Maokou Group		P_2m	>180			The lithology is mainly medium-thick to thick limestone, with a regional thickness of 181. 258 m, which is not exposed in the mining area. Cracked cave water, underground The runoff modulus is $4-10L/S \cdot km^2$. Strong water-rich, strong water layer.

Fig. 1. Hydrogeology of mining area.

morphology is irregular, with a maximum extension of about $30 \mu m$. The micro-holes are more developed, and the size of the holes is about $2-6 \mu m$. C is sandstone, its rock is dense, local development of micro-cracks, fracture morphology into a linear, the maximum extension of about $35 \mu m$, micro-holes are more developed, the size of the hole is about $3-8 \mu m$; D is mudstone, its rock is dense, local development of micro-cracks, crack shape into a linear, the maximum extension of about $12 \mu m$, no micro-holes found; E is argillaceous siltstone, the rock is dense, local development of micro holes, hole size is about $1-3 \mu m$; F is limestone, its rock is dense, local development of micro-cracks, irregular fracture morphology, the maximum extension of about $20 \mu m$, micro-holes are more developed, the size of the hole is about $2-8 \mu m$. The observation results show that the primary cracks in the overlying strata of the coal seam roof are not developed.

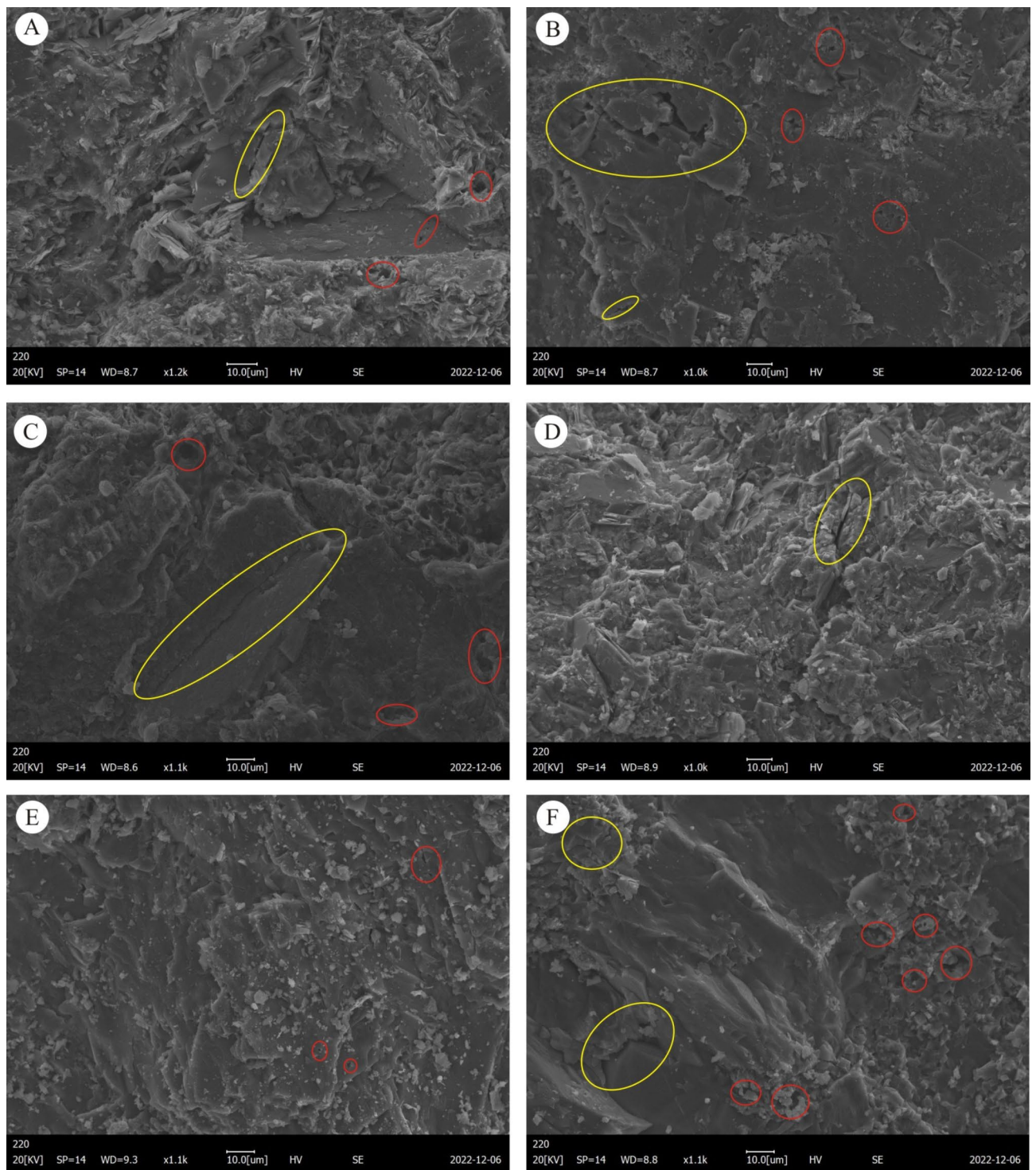


Fig. 2. Microscopic characteristics of roof overburden rock.

Analysis of macroscopic structural characteristics of overlying strata rock

Most of the coal-bearing rock series in Longfeng Coal Mine belong to concealed strata, and only some outcrops are exposed on the surface. Therefore, the boreholes are systematically observed. It is found that the rock bedding is developed, the fissures are not developed, and the rock is relatively dense and complete. Through the statistics of the core recovery rate of the boreholes between the top of No.9 coal seam and Changxing Formation in Longfeng Coal Mine, the recovery rate is high, indicating that the rock integrity is good, and the core recovery rate distribution is as shown in Fig. 3.

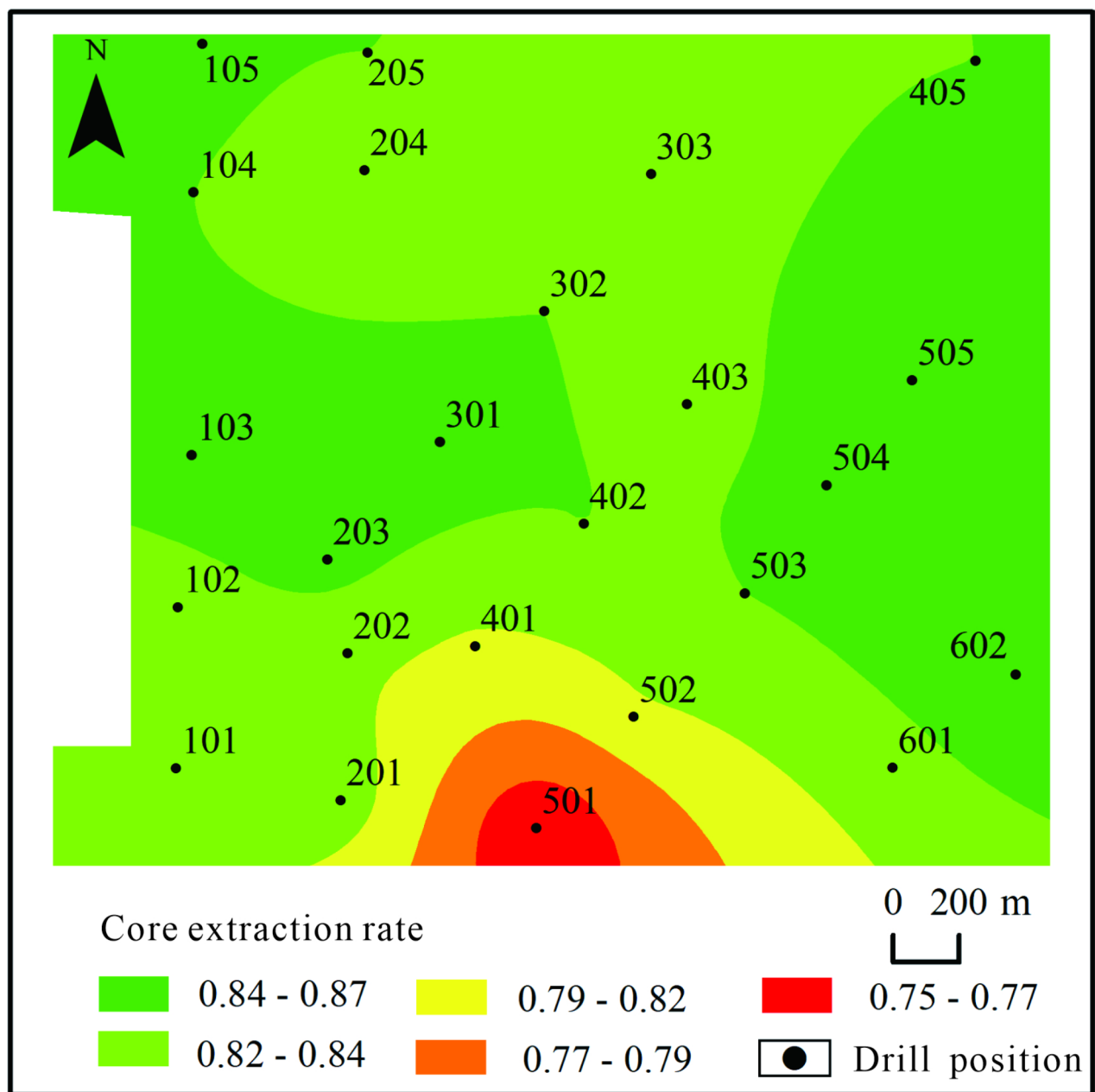


Fig. 3. Distribution of core extraction rate.

Physical and mechanical parameters test of overlying strata rock

The rock physical and mechanical properties of overlying strata are important factors affecting the failure law of roof overlying strata and inducing mine water inrush accidents, and are also the premise of accurately constructing numerical simulation models. Therefore, a specific location in the working face was selected for drilling sampling, and a series of rock mechanics parameter test tests were carried out indoors. The test was carried out on the RMT-301 rock mechanics test system. Three standard rock specimens were prepared for each lithology for testing, and the average value was taken as the test result. The axial load of the testing machine is controlled by displacement loading, and the loading rate is 0.005 mm/s. The test results are shown in Table 1.

Methodology

Basics of key stratum

Position analysis of roof hard rock stratum

In the process of coal seam mining, the relatively hard and thick rock strata are usually used as the main bearing body in the overburden rock, which controls the load transfer and interaction between the rock strata of the overlying rock mass. The key stratum controls the activity of the overlying rock layers in the excavation working

Lithology	Compressive strength (Mpa)	Modulus of elasticity (Gpa)	Poisson's ratio	Cohesion (Mpa)	Internal friction (°)	Tensile strength (Mpa)
Siltstone	44.55	18.50	0.29	3.80	39.50	2.39
Fine sandstone	50.75	38.70	0.28	3.70	38.90	8.06
Mudstone	18.50	11.90	0.20	1.40	34.10	1.59
Silty mudstone	29.30	14.90	0.21	2.90	27.20	2.57
Argillaceous limestone	37.50	26.40	0.20	3.70	41.50	3.87
Limestone	42.20	40.00	0.20	4.00	40.30	8.80

Table 1. Rock test results of overlying strata.

face and even all the rock layers up to the surface²⁷. The fracture of the key stratum will affect the deformation and failure of the roof overburden rock^{28–32}.

According to the theory of “key stratum”, the load of the strata adjacent to the coal seam is calculated first, and the first layer of hard rock is determined. When the first layer to the mth layer of the upper part of the first layer of hard rock moves and deforms, while the m + 1st layer of rock does not deform, the m + 1st layer of rock is the second layer of hard rock of the roof overburden, and so on to obtain all the hard rock in the mining roof overburden.

The load of the first layer of hard rock is :

$$(q_n)_1 = \frac{E_1 h_1^3 \sum_{i=1}^n h_i \gamma_i}{\sum_{i=1}^n E_i h_i^3} \tag{1}$$

where $(q_n)_1$ is the load of the nth stratum to the hard stratum, Mpa; h_i is the thickness of the i-th rock layer, m; γ_i is the bulk density of the ith stratum, MN/m³; E_i is the elastic modulus of the i-th rock layer, GPa.

Calculation of fracture distance of roof hard rock stratum

After determining the position of the hard rock strata in the roof of the working face, it is also necessary to calculate whether the hard rock strata meet the strength conditions of the key stratum. In the process of coal seam mining, before the hard rock stratum of the roof breaks down, both ends are supported by the coal walls on the left and right sides. At this time, the key stratum can be regarded as a “fixed beam” to calculate the fracture step of the rock stratum. Then the fracture step L_s of the hard rock stratum of the sth layer can be calculated by Eq. (2).

$$L_s = h_s \sqrt{\frac{2R_s}{(q_n)_s}} \quad (s = 1, 2, \dots, k) \tag{2}$$

where h_s is the thickness of the s-th hard rock layer, m; R_s is the tensile strength of the sth layer of hard rock, MPa; $(q_n)_s$ represents the load from the n-th layer on the s-th layer of hard rock, MPa.

Numerical simulation

The model applied in the present study was established using FLAC3D and represents the geological prototype of the 120,905 working face in Longfeng Coal Mine. This working face concentrates on the No. 9 coal seam at a depth of 200–300 m and dip angle of 6°. Given the near horizontal dip angle, its influence on the coal seam is not considered. The model represents an area of 480 m × 240 m × 150 m, comprising 385,000 units. The boundary effect was negated by setting a 70-m protective coal pillar around the working face. The coal seam excavation in the model was designed to have a once-off full mining height and excavation at 10 m per step for 20 steps. Roof support was not represented in the numerical model to increase the probability of overburden failure due to coal seam mining. The natural caving method was included in the model to manage the roof to ensure that an empty space is formed after mine excavation. The model represented the upper mine stratum by applying the upper load. Displacement constraints were applied in the front-back, left-right, and bottom directions of the model. As shown in Table 1, the results of the physical tests confirmed the assignment of rock layers in the numerical model. Figure 4 shows the conceptual structure of the established numerical model.

Engineering measurement analysis

The present study integrated the high-density electrical and borehole imaging fine detection methods to detect and analyze the height of the water-conducting fracture zone of the mining roof of the working face, with the results verified against the 120,905 working face of Longfeng Coal Mine.

The high-density electrical method uses the E60D high-density electrical instrument to survey the deformation and failure of the rock layer according to the electrical sounding method. The electrical sounding method mainly increases the measurement depth by gradually increasing the power supply electrode distance, so as to obtain the variation law of the apparent resistivity value from the surface to the coal mining face in the vertical direction. Through the analysis of the electrical sounding phAs curve, the characteristics of the deep geological section from the surface to the mine can be obtained. In the electrical sounding method, symmetrical quadrupole devices are commonly used, as shown in Fig. 5 (a). During the detection, the ratio of the power

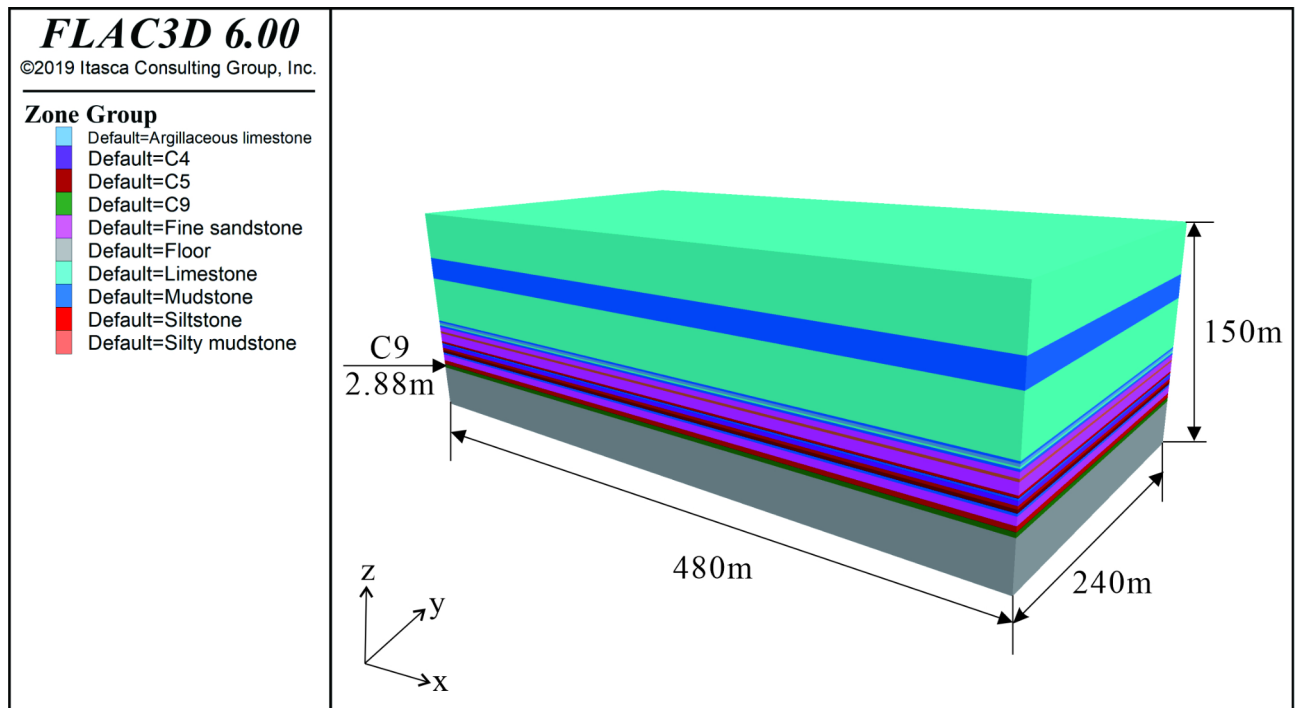


Fig. 4. Numerical model.

supply electrode to the measurement electrode gradually increases from a certain value. Each time the power supply electrode changes, a ΔU_{MN} and I_{AB} are output correspondingly, and then the resistivity value of each point is calculated. Using the double logarithmic coordinate system, according to the resistivity value of the measuring point, taking 0.5 times of the power supply electrode as the abscissa, and the resistivity value of the measuring point as the ordinate, the high-density electrical sounding curve is drawn, as shown in Fig. 5(b). When the water-conducting fracture zone and the upper aquifer are connected and the groundwater enters the goaf along the water-conducting fracture zone, the water-conducting fracture zone is water-bearing, and its electrical performance is relatively low resistance. When the water flowing fractured zone and the water without aquifer or aquifer above have entered the goaf through the water flowing fractured zone, the water flowing fractured zone is weakly water-bearing, and its resistivity is relatively high. Therefore, the change of resistivity value in the measured area is measured by E60D high-density electrical instrument, and the development height of water-conducting fracture zone can be inferred.

Borehole imaging uses CXK12 mine borehole imager. Based on DSP technology, the internal conditions of the borehole are observed and the borehole trajectory is tracked. The borehole trajectory map and three-dimensional core map are automatically generated to form a digital borehole core. In the measurement, the depth counter and the probe play a key role. The probe captures the hole wall image through its built-in LED white light emitting diode and camera, and the depth counter records the depth of the probe. The image signal and the probe signal are transmitted to the host through the transmission cable, and the host calculates the position of the probe according to the received signal.

Results and discussion

Determination of key stratum and analysis of fracture characteristics

Determination of key stratum of roof overburden in working face

Based on Eqs. (1) and (2) and the composition of the overlying rock layers on the working face, it can be judged that the second layer of 4.90 m thick fine sandstone, the ninth layer of 6.57 m thick fine sandstone, the 16th layer of 33.00 m thick limestone, and the 18th layer of 129.55 m thick limestone above the 120,905 working face are hard rock layers, and the breaking step distance is 34.62 m, 41.92 m, 121.89 m, 1526.76 m respectively. Because the mining length of the working face is 590 m, which is less than the fracture step distance of the 18th stratum, the 18th stratum will not break during the mining process of the working face.

From the above, it can be judged that the second layer of rock is a inferior key stratum, the 16th layer of rock is the main key stratum, the 9th layer of rock and the 18th layer of rock are the key stratums, and the distribution of the roof of the working face is shown in Fig. 6.

Analysis of fracture characteristics of key stratum in roof overburden rock

According to the above calculation, the second layer of 4.90 m thick fine sandstone above the 120,905 coal mining face is the main roof, which controls the deformation and fracture of the rock strata within the range of 10.36 m above it. After the open-off cut of the coal seam, the direct roof of the working face will gradually

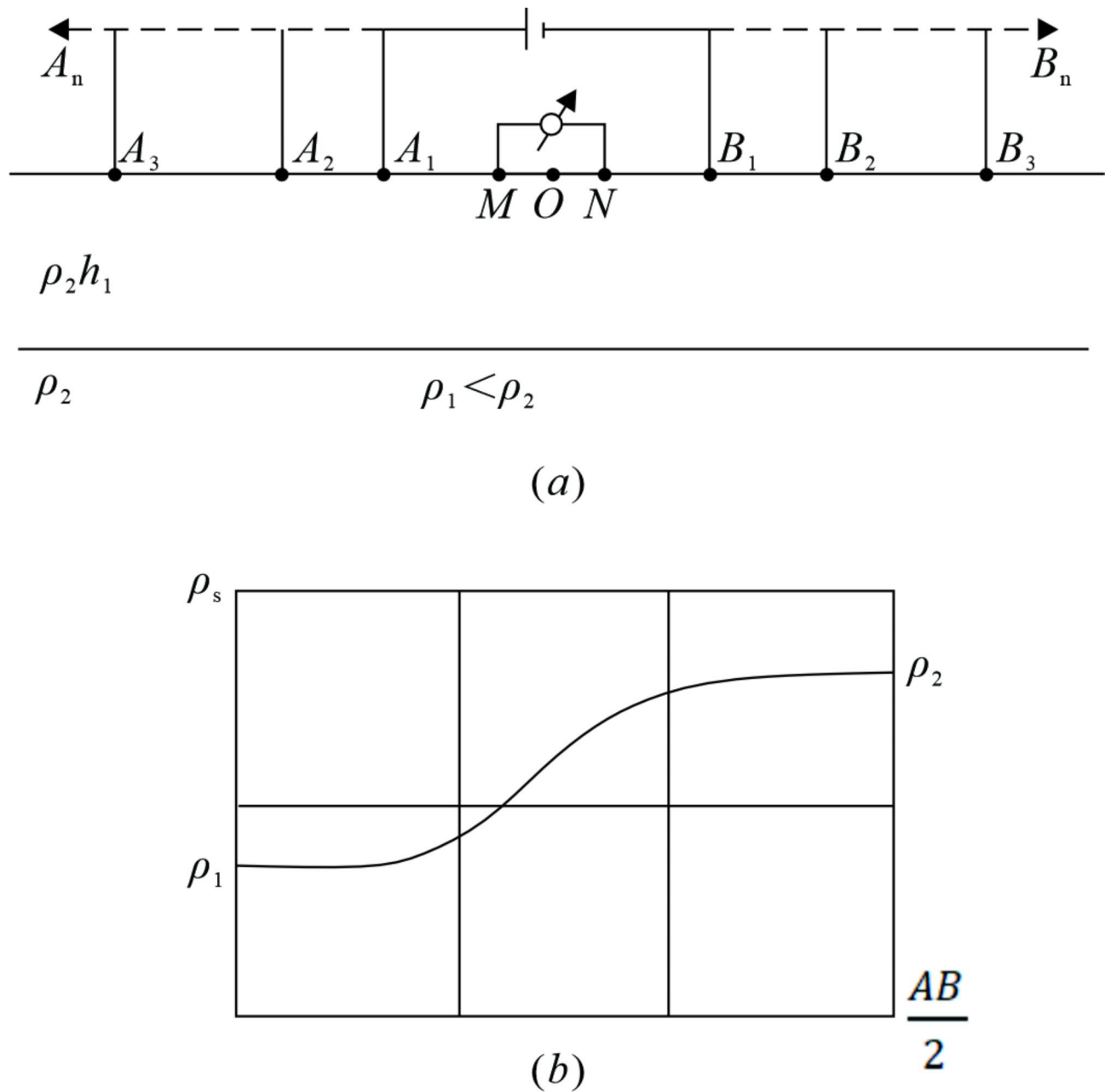


Fig. 5. Working principle of high density electrical method.

collapse in a suspended state due to the influence of the advancing distance of the working face. When the suspended distance of the main roof reaches the limit breaking step, the fracture will occur, and the rock strata controlled by it will deform and sink synchronously in the range of 10.36 m above it.

Affected by the deformation and subsidence of the main roof, the supporting point of the suspended main roof moves forward and backward. At this time, the state of the main roof rock beam is between the fixed beam and the simply supported beam³³. Combined with the actual geological conditions of the 120,905 working face, two kinds of rock beam models are established, and the mechanical analysis is carried out. The mechanical model is shown in Fig. 7. The mechanical analysis of the two beam structure models is carried out, and the ultimate breaking step distance of the key stratum of the basic roof is about 40.86 m. Under the mining disturbance, the key stratum of the basic roof will be broken and accompanied by the formation of water-conducting fissures³⁴. The water-conducting fissures will continue to develop upward, but the final development height remains to be determined.

Overburden stress field evolution law

Each rock mass structure is in a state of stress equilibrium under natural stress. Due to the formation of goaf after coal seam excavation, the equilibrium state of rock mass is destroyed and the stress changes. With the continuous

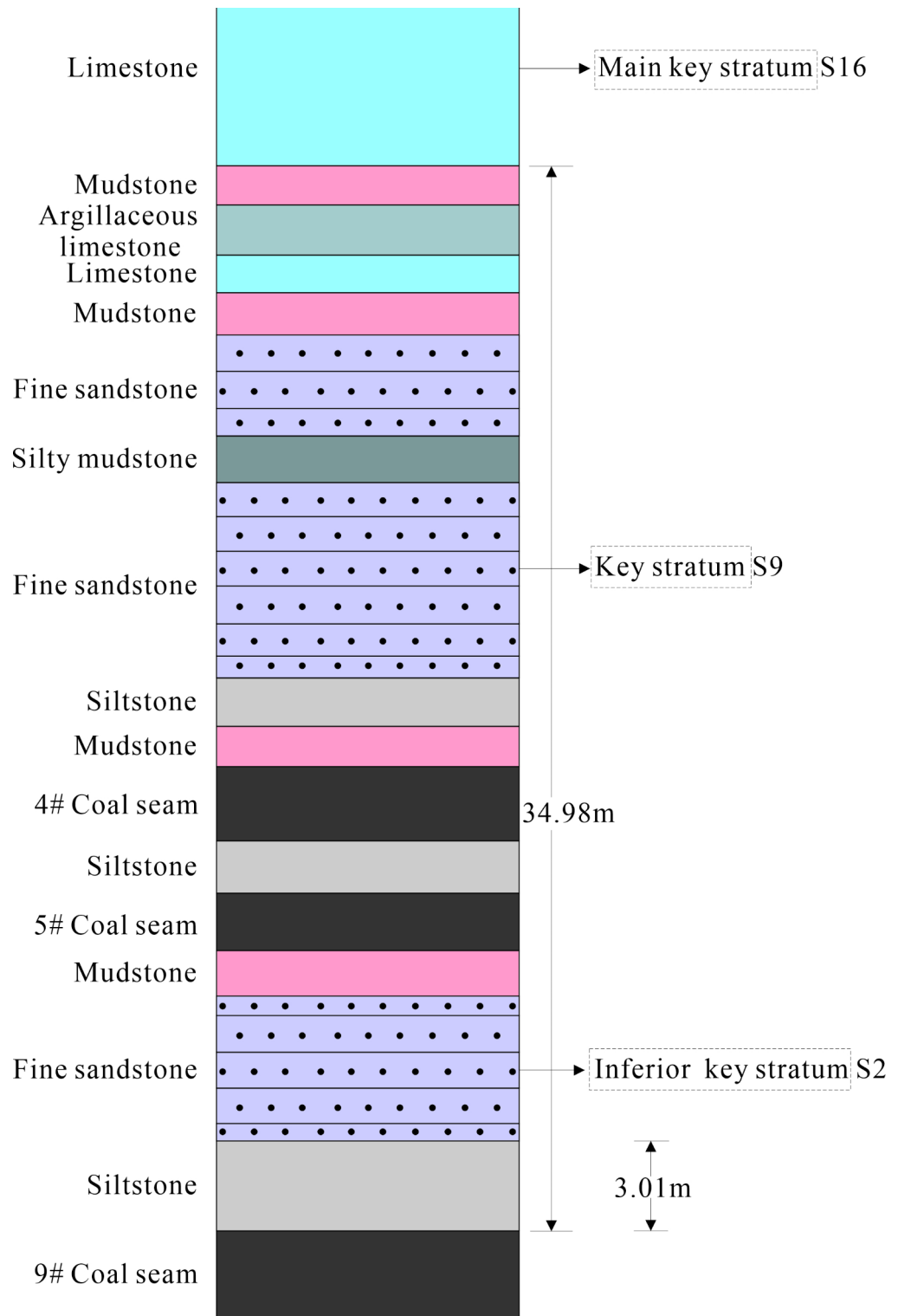


Fig. 6. Key strata distribution of roof.

advancement of coal mining face, the goaf is expanding. When the stress state of the rock mass exceeds the load limit it can withstand, collapse will occur. Therefore, it is necessary to analyze the stress variation law of overlying strata of coal seam roof under different advancing distances of working face. The numerical simulation results are shown in Fig. 8.

Figure 8 shows the evolution process of the vertical stress of the overlying strata of the coal seam when the working face advances to 50 m, 80 m, 110 m, 140 m, 170 m and 200 m. When the working face is advanced to 50 m, there is a pressure relief zone on the roof and floor of the goaf, and a small pressure relief arch appears

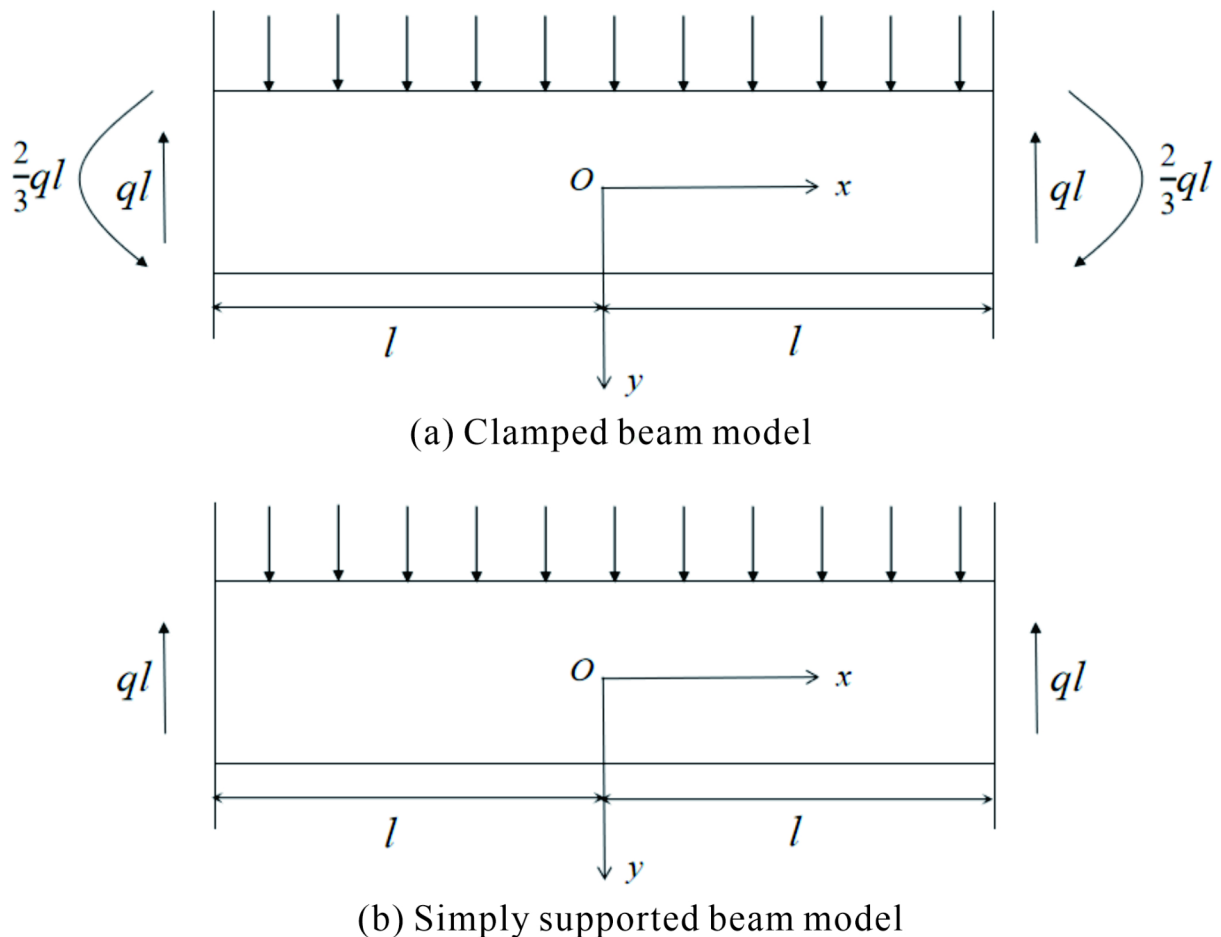


Fig. 7. Mechanical analysis model of key stratum of overburden rock.

above the coal mining face, and it continues to expand upward in the vertical direction. The vertical stress of the roof overburden is symmetrically distributed with the midpoint of the goaf as the symmetrical center. This shows that the rock strata adjacent to the goaf collapses, and stress concentration occurs at the open-off cut and the stop line, and the maximum concentration stress value is about 16.8 MPa; when the working face advances to 80 m, the influence of coal seam mining on the stress distribution of overlying strata is more significant. The main roof of the working face further collapses, and the pressure relief area extends to the rock strata above the main roof. The vault is relatively high above the goaf, and the overburden stress is symmetrically distributed along the arch axis. The stress concentration appears at both ends of the goaf, and the maximum concentrated stress value is about 17.9 MPa. When the working face advances to 110 m away from the open-off cut, the pressure relief zone extends upward and forward. The pressure relief arch above the goaf is still symmetrically distributed along the arch axis, and the stress concentration value at the open-off cut and the stop line increases to 18.5 MPa. When the working face advances to 140 m, there is still a pressure relief arch above the goaf and the stress concentration still appears at the end of the goaf, and the maximum concentrated stress value is 19.0 MPa. When the working face is advanced to 170 m, the pressure relief arch continues to expand forward, and the maximum concentrated stress value is 19.3 MPa; when the coal mining face is excavated to 200 m, with the subsidence, collapse and compaction of the overlying strata of the coal seam mining roof, the pressure in the pressure relief area is gradually stabilizing, and the stress balance of the overlying strata in the goaf will be re-established. At this time, the maximum concentrated stress value at both ends of the goaf is 19.4 MPa.

The key stratum of overlying strata in the 120,905 coal mining face were identified as fine sandstone and limestone 3.01 m, 18.27 m, 34.98 m, and 83.72 m away from No.9 coal seam. Therefore, the monitoring line was arranged horizontally on the upper surface of the key layer S2 and the key layer S9 to represent the basic roof, whereas the lower left corner of No.9 coal seam was set as the origin. Given that the protective coal pillar was set at 70 m, the starting point in the x-direction is 70, and the endpoint is 270. To make the observation results more precise, the midpoint in the y-direction was selected, which is 120. The z-direction is defined as the total thickness of the coal and rock layers above the coal seam base and below the upper surface of key layers S2 and S9. Thus, The starting and end points of line S2 were set as (70,120,10.79) and (270,120,10.79), respectively; those of survey line S9 were set as (70,120,70.86) and (270,120,70.86), respectively. A monitoring point was

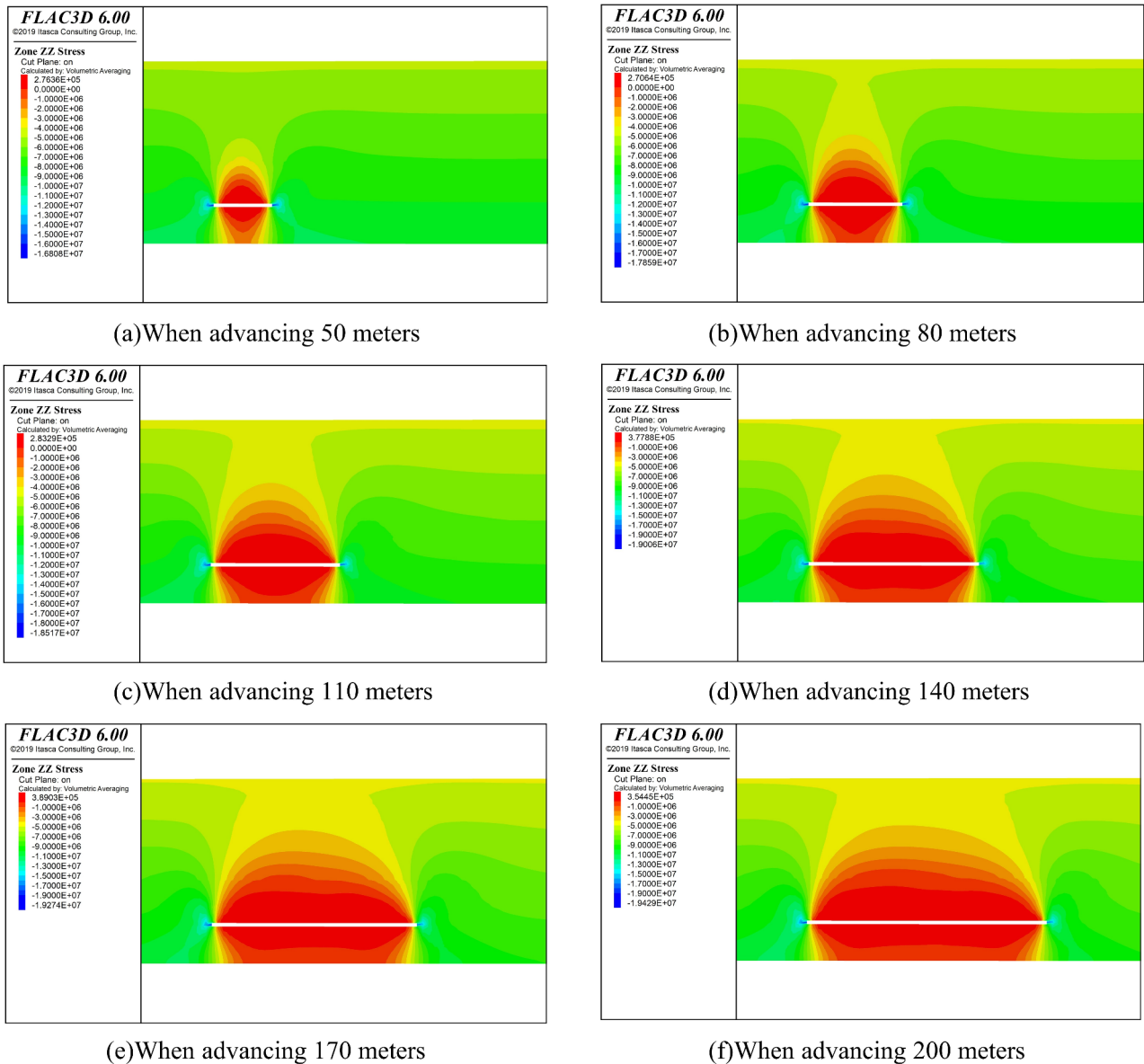


Fig. 8. Evolution law of stress field of overlying strata in coal seam mining roof.

arranged every 10 m of the monitoring line, consistent with each excavation extending for 10 m, for a total of 21 monitoring points. These monitoring points were used to monitor changes in vertical stress in the roof under different advancing distances of the working face.

According to the vertical stress data obtained from the monitoring line distributed above, the vertical stress variation curve of the roof under different advancing distances of the working face is drawn as shown in Fig. 9.

Figure 9 (a) and (b) are the vertical stress evolution diagrams of the monitoring points of the two survey lines. The abscissa represents the excavation step distance, the ordinate represents the vertical stress, the negative value represents the tensile stress, the positive value represents the compressive stress, and the curve represents the stress of each monitoring point when the excavation is at a certain distance. It can be seen from Fig. 9 (a) that after the excavation of the coal seam, the S2 pressure of the key stratum of the immediate roof is maintained at about 1.7Mpa. As the working face advances, the peak stress in front of the working face gradually increases from 9.28Mpa to 11.1Mpa, and the longer the advancing distance, the smaller the influence of mining disturbance on the front of the working face, indicating that the mining face gradually tends to be stable. The peak stress at the key stratum S9 is smaller than the direct peak stress, and there is a certain lag, as shown in Fig. 9 (b). This is mainly related to the stability of the key stratum structure. On the whole, the vertical stress change law at the key stratum S9 is similar to the vertical stress change law of the direct roof, but the stress peak curve is more gentle due to the pressure relief of the direct roof.

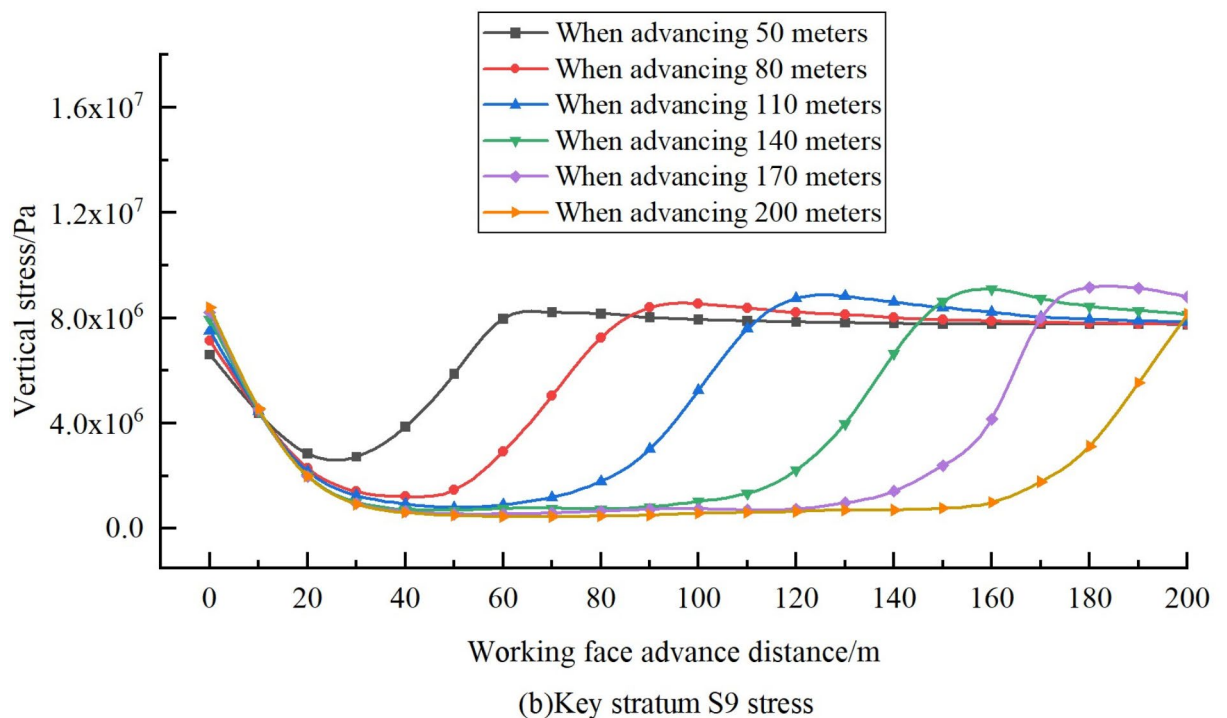
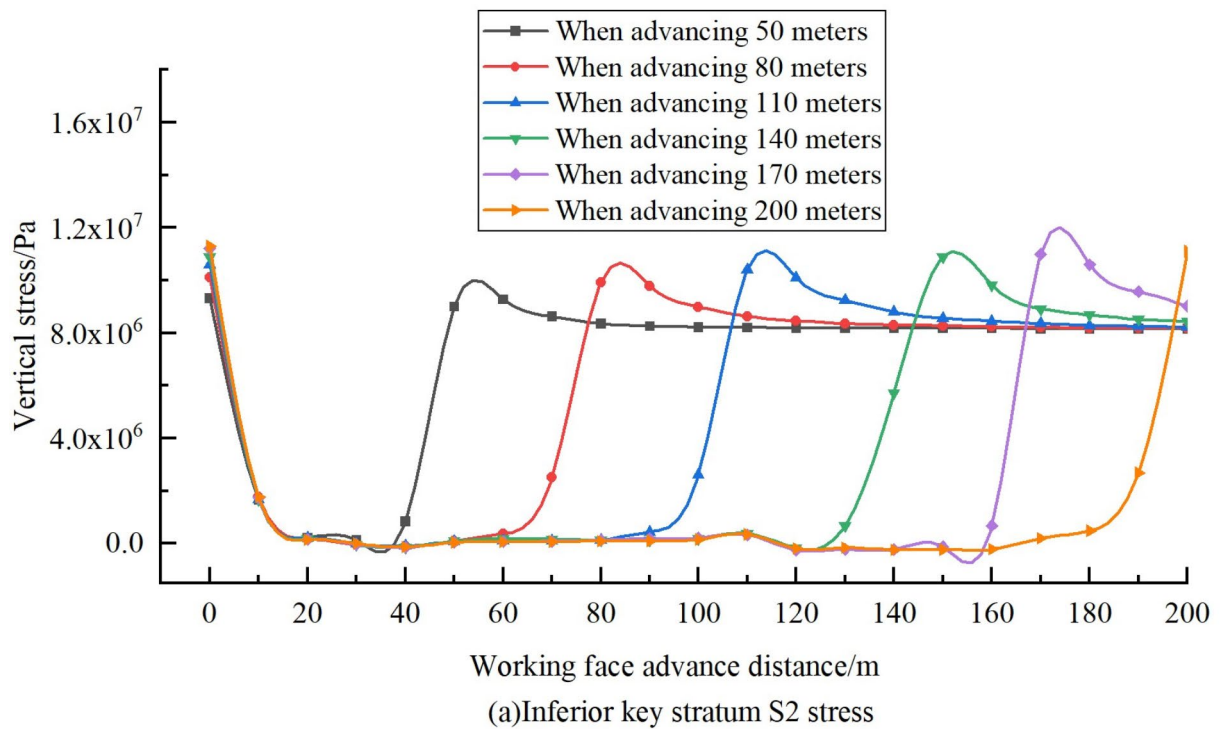


Fig. 9. Stress variation law at different advancing distances of working face.

Evolution law of overburden rock displacement field

After the coal seam is mined, with the continuous excavation of the working face, the overlying strata are continuously destroyed, and the overlying strata of the roof gradually deform, sink, collapse, and compact to the goaf, so that the space of the goaf is gradually reduced, and the caving zone, fracture zone and bending subsidence zone are formed from the bottom to the top of the goaf, and the bottom drum appears on the floor. Through the numerical simulation results, the migration and evolution law of overlying strata of coal seam mining roof under different advancing distances of working face is analyzed and summarized, as shown in Fig. 10. The diagram

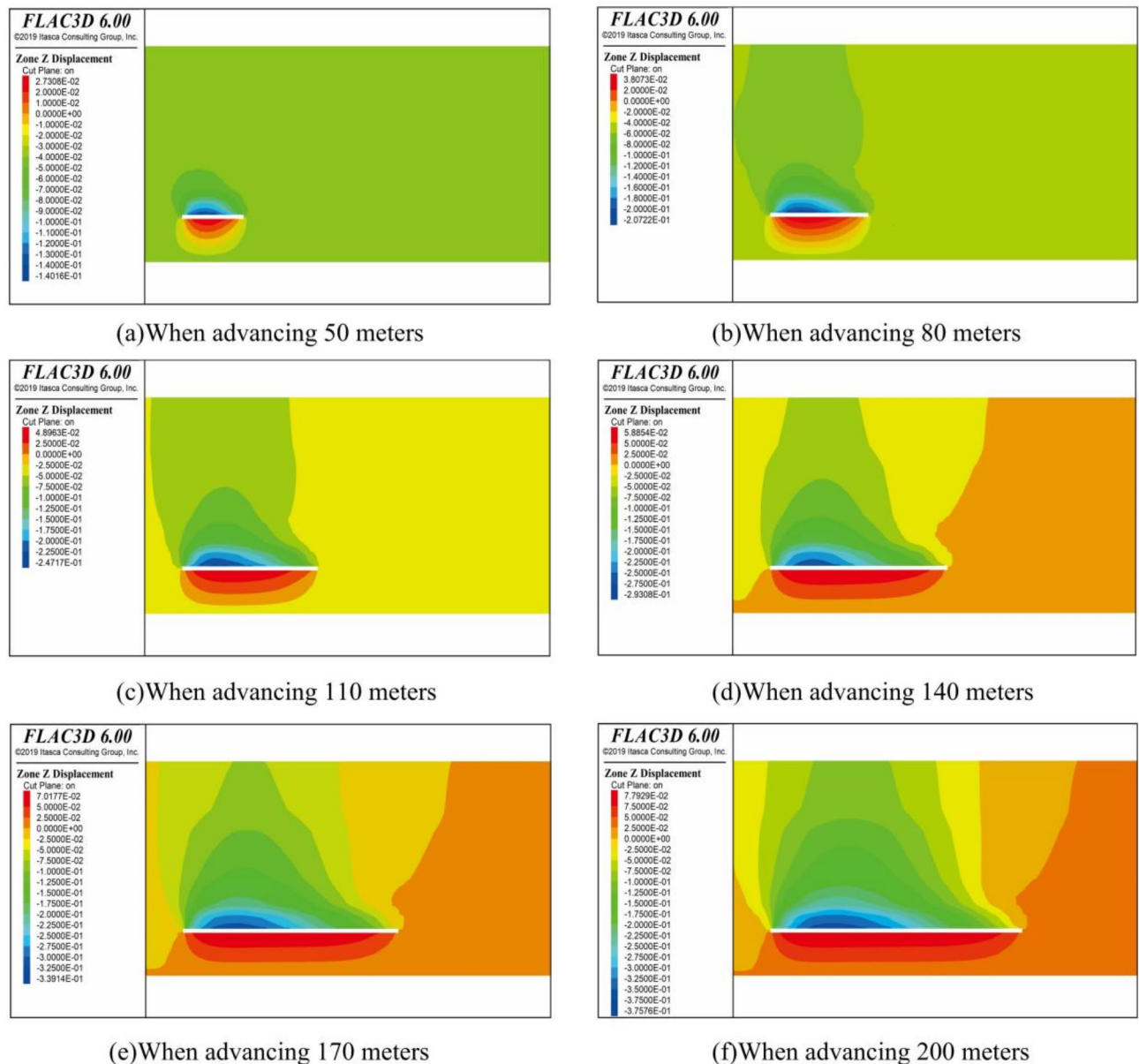


Fig. 10. Evolution law of displacement field of overlying strata in coal seam mining roof.

shows the evolution process of vertical displacement of overlying strata in coal seam mining when the working face is advanced to 50 m, 80 m, 110 m, 140 m, 170 m and 200 m. It can be seen that with the advancement of the working face, the strata adjacent to the working face sink, and the amount of subsidence increases with the increase of the advancing distance, and the displacement cloud map shows an “arch” shape. At the same time, under the influence of the extrusion of the confined rock strata on both sides, the floor heave occurs below the goaf, and the displacement value of the floor heave also increases with the increase of the advancing distance.

Evolution law of plastic zone of overlying strata

The dynamic process of overburden movement, deformation and failure during coal seam excavation and the prediction of the development height of roof water-conducting fracture zone are obtained by FLAC3D simulation. It is mainly based on the fact that the overlying strata of coal seam roof will have certain tensile or shear failure under the influence of mining disturbance, thus showing the characteristics of failure zone in the model. Therefore, the development height of the water flowing fractured zone can be obtained by analyzing the evolution of the plastic zone of the overlying rock of the coal seam roof under different advancing distances of the working face, as shown in Fig. 11.

Figure 11 shows the distribution of the plastic zone of the overlying strata of the coal seam mining roof when the working face is advanced to 50 m, 80 m, 110 m, 140 m, 170 m and 200 m. The failure range of the plastic zone of the overlying strata of the mining roof continues to expand with the increase of the advancing distance

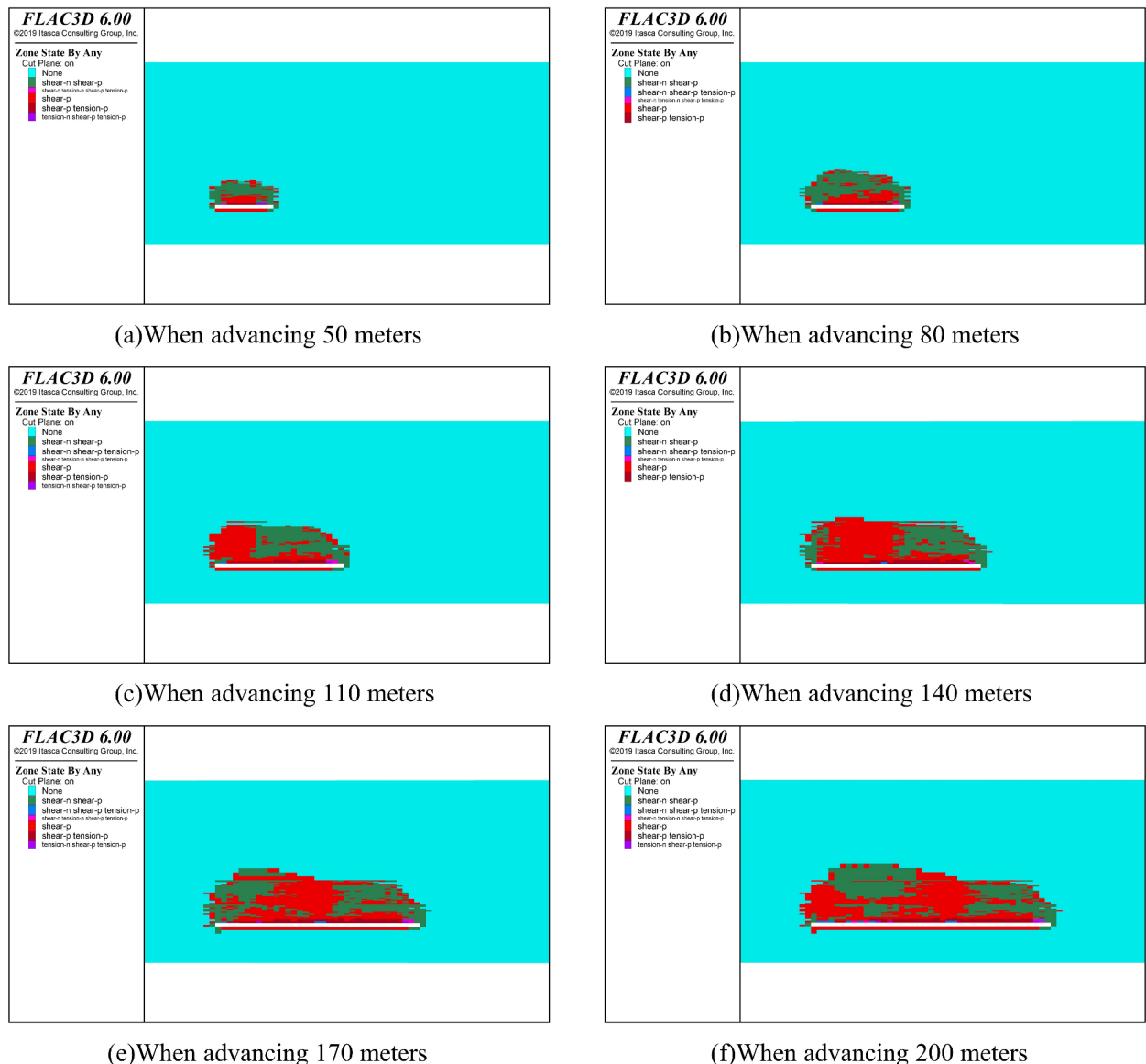


Fig. 11. Evolution law of plastic zone of overlying strata in coal seam mining roof.

of the working face. When the coal mining face is excavated to 50 m, due to the emergence of the goaf, the roof rock layer is deformed and destroyed. The upper rock layer immediately adjacent to the working face is first subjected to tensile failure. The height of the plastic zone is 19.61 m, and it continues to develop upward. When is advanced to 80 m, the plastic failure in the middle of the goaf is more serious. Shear failure occurs along the side of the mining eye and the side of the stop line above the working face, and extends to the mudstone. The plastic failure zone begins to show a classic “trapezoid” shape, and the height of the plastic zone is 26.38 m. When mining to 140 m, the shear failure at 34.98 m above the working face extends from the middle to the side of the mining eye and the stop line, and because the advancing distance is greater than the breaking step of the main key stratum at this time, the shear deformation of the main key stratum S16 begins to occur, and the height of the plastic zone is 38.27 m. When the working face advances to 170 m, the plastic zone on the left side of the upper part continues to extend horizontally and vertically, and the failure height of the plastic zone of the roof begins to stabilize. At this time, the height of the plastic zone is 42.21 m. When the working face advances to 200 m, the lateral development of the plastic zone is more obvious than the longitudinal development. At this time, the maximum development height of the plastic zone is 46.12 m.

Analysis of development height of water flowing fractured zone

When using numerical simulation software to study the failure law of roof overburden under different advancing distances of working face, in order to be closer to the failure of overburden after coal seam mining in engineering practice, roof support has not been designed in numerical simulation. Therefore, in the process of expanding

the scope of goaf, the corresponding stress concentration area is bound to be formed in the process of roof overburden failure caused by coal seam mining.

The plastic zone in FLAC3D represents the area in which tensile or shear failure in the rock mass produces cracks. According to the stress field and plastic zone conceptually represented in Figs. 8 and 11, these can occur through loss of the lower support of the roof overburden due to excavation of the coal seam. During this process, redistribution of the overburden results in the gradual release of pressure by the weight of the rock layer. Fracture and collapse occur in each rock layer when the limit to breaking step distance is exceeded. Corresponding to the numerical simulation, the stress of the overburden changes and the rock layer is destroyed. The plastic zone of the roof overburden develops horizontally and vertically with the expansion of the goaf range. With the increase of the advancing distance of the working face, the damage area above the goaf gradually expands, and the vertical stress distribution of the overlying strata of the coal seam roof changes. With the increase of the excavation step distance of the working face, the goaf continues to advance, and the stress and displacement in the vertical direction of the overlying rock show a “rapid increase-slow increase”, indicating that the initial damage of the overlying rock of the mining roof is more severe. Then, as the overlying rock layer breaks and falls gravel, it gradually fills and compacts the rear of the goaf, and the vertical stress and vertical displacement of the overlying rock of the mining roof slow down.

In the prediction of the height of the water flowing fractured zone by numerical simulation, the “plastic zone” method and the “principal stress” method are commonly used to judge the development height of the water flowing fractured zone^{35–37}. The former determines the maximum height of the water-conducting fracture zone according to the range and height of the plastic failure zone, while the latter determines the height of the water-conducting fracture zone according to the distribution of the maximum and minimum principal stresses. The present study applied the plastic zone method, represented in FLAC3D as the area in which the rock mass undergoes tensile or shear failure to produce cracks. The vertical height of the plastic zone area represented the height of the water-conducting fracture zone. The volume of the plastic failure zone was calculated by FLAC3D, following which the development height of the water-conducting fracture zone was determined by combining the vertical height of the plastic zone (see Fig. 12 for the results).

As shown in Fig. 12, the advancing distance of the working face directly affects the development of the water-conducting fracture zone, which can be divided into three stages: (1) slow growth; (2) rapid growth; (3) stable growth. After completion of the open-off cut of the coal seam, the roof overburden is sporadically damaged, resulting in a few cracks. When the working face advances from 0 m to 30 m, the overburden failure gradually appears. Because the key stratum S2 of the roof overburden has a certain supporting effect on the upper rock layer, the development of the water-conducting fracture zone is inhibited, and the longitudinal extension speed

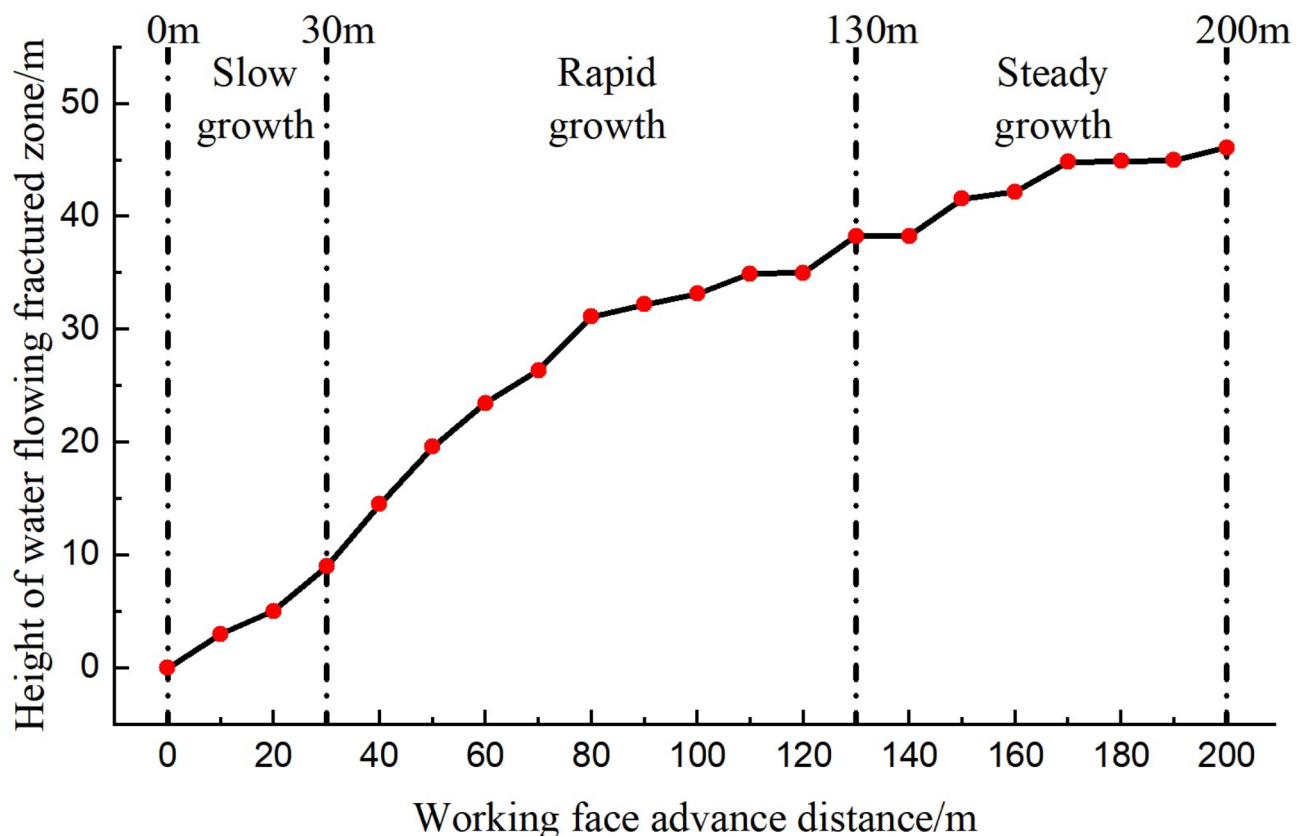


Fig. 12. Development height of water flowing fractured zone of roof overburden rock.

is relatively slow. At this time, the water-conducting fracture zone is slowly developed. When the working face advances from 30 m to 130 m, affected by the fracture of key stratum S2, S9 and S16, the fracture of overlying strata on the roof extends upward rapidly, and the height of water-conducting fracture zone increases suddenly, from 8.99 m to 38.27 m. After 130 m, the fracture instability of the main key stratum S16 may lead to the occurrence of dynamic water inrush accident. With the release of the kinetic energy of the main key stratum, the height of the water-conducting fracture zone tends to be stable, and the final height of the water-conducting fracture zone is 46.12 m.

Measured analysis of development height of water flowing fractured zone

While the current study conducted a relatively detailed examination on the development height of the water-conducting fracture zone, the practical significants of the results for guiding engineering need to be validated. These results were validated against the 120,905 working face of Longfeng Coal Mine using the integrated high-density electrical and borehole imaging methods to detect and analyze the height of the water-conducting fracture zone of the mining roof of the working face.

The high-density electrical method uses the E60D high-density electrical instrument to survey the deformation and failure of the rock layer according to the electrical sounding method. The change of resistivity value in the measured area is measured by E60D high-density electrical instrument, and the development height of water-conducting fracture zone can be inferred. This survey is based on the survey line, and all the data obtained from the survey line are systematically analyzed. It is found that the fracture height is 42–44 m.

Borehole imaging uses CXK12 mine borehole imager. The arrangement of the observation hole of the borehole imager should first consider whether the position of the observation hole of the borehole imager can detect the highest point of the “trapezoid”, which is the development form of the overlying rock fracture zone of the mining roof. Based on the empirical formula and numerical simulation calculation, a borehole is arranged in 120,905 working face to predict the development height of water flowing fracture in overlying strata of mining roof. The CXK12 borehole imager was used to observe the borehole in real time, and the camera was peeped for 26 min. The actual detection hole depth was 58.2 m. By watching the video repeatedly, the more representative segments are intercepted as the detection results for analysis. The main snooping results are shown in Fig. 13. It can be seen from Fig. 13 that the borehole imager probe has a crack at 0.8 m into the hole, the rock is broken, and there is crack development. The hole depth is 0.8 m ~ 58.1 m, the internal cracks of the rock layer are developed, and the average elevation angle of the borehole is 70°. According to the trigonometric function transformation, the hole depth of 0.8 m ~ 55.1 m corresponds to the upper part of the coal seam of 0.7 m ~ 51.8 m. Combined with the spatial distribution of the overlying strata on the roof borehole histogram, it shows that the water-conducting fracture of the overlying strata has penetrated the bottom of the overlying Changxing Formation aquifer, but has not penetrated the entire aquifer. Since the hole depth is 55.1 m, the cracks on the hole wall gradually decrease, and the probe continues to advance to the deep part. The deep hole wall is relatively complete and smooth, and there is no crack, indicating that the water-conducting fracture reaches the maximum extension height at the hole depth of 55.1 m. The vertical height of the water-conducting fracture is 51.8 m by trigonometric function transformation.

Discussion

Application of comprehensive detection technology identified the maximum development height of water-conducting fracture in the mining roof to be between 42 m and 51.8 m, while the maximum height of the water-conducting fracture zone obtained by numerical simulation was 46.12 m, in the range of measurements. The above result confirms that the plastic zone method is reliable for characterizing the evolution of water-conducting fractures. The results of the present study can help improve the predictions of height and the measurements of water-conducting fracture zones in coalfields in northern Guizhou. The distance of 34.98 m between the bottom of the aquifer in the overlying Changxing Formation of the coal seam from the top of the No.9 coal seam indicates that the water-conducting fracture of the overlying strata of the mining roof interacts with the aquifer in the overlying Changxing Formation of the roof, contributing to risk of water inrush.

There are also cases internationally where numerical simulations have been used to confirm the height of the water-conducting fracture zone. For instance, at the International European Rock Mechanics Symposium in Russia, the numerical simulation results for the formation height of the water-conducting fracture zone during mineral extraction were discussed. The results indicate that using numerical simulations to assess the height of the water-conducting fracture zone is feasible, and that the formation height is closely related to the length of the goaf, coal seam thickness, and rock mechanics properties³⁸. The technology can quickly obtain on-site information from the mining area, providing a basis for the design of waterproofing measures.

Conclusions

(1) The high recovery rate of each rock layer indicates good integrity of the overlying rock layer. The primary fissures of all rocks types in the overlying strata of No.9 coal seam were undeveloped, indicating that the water flowing fissures in the overlying strata of the roof are undeveloped in the natural state.

(2) Overlying strata of the No.9 coal seam roof have predominantly hard outer layers encompassing a soft inner layer. Four key strata were identified in the roof of 120,905 coal mining face: (1) fine sandstone (thickness of 4.90 m, 3.01 m above No.9 coal seam); (2) fine sandstone (6.57 m; 18.27 m); (3) limestone (33 m; 34.98 m); (4) limestone (129.55 m; 83.72 m). After introducing the beam structure, the ultimate breaking step distance of the key stratum of the basic roof was 40.86 m.

(3) Highest stress concentrations were identified at the mining shaft and the stop line of the working face. Pressure and energy release of the upper strata in the goaf contributed to generally low and high stress distributions in the middle and ends, respectively. The goaf increases with continuous advancement of the

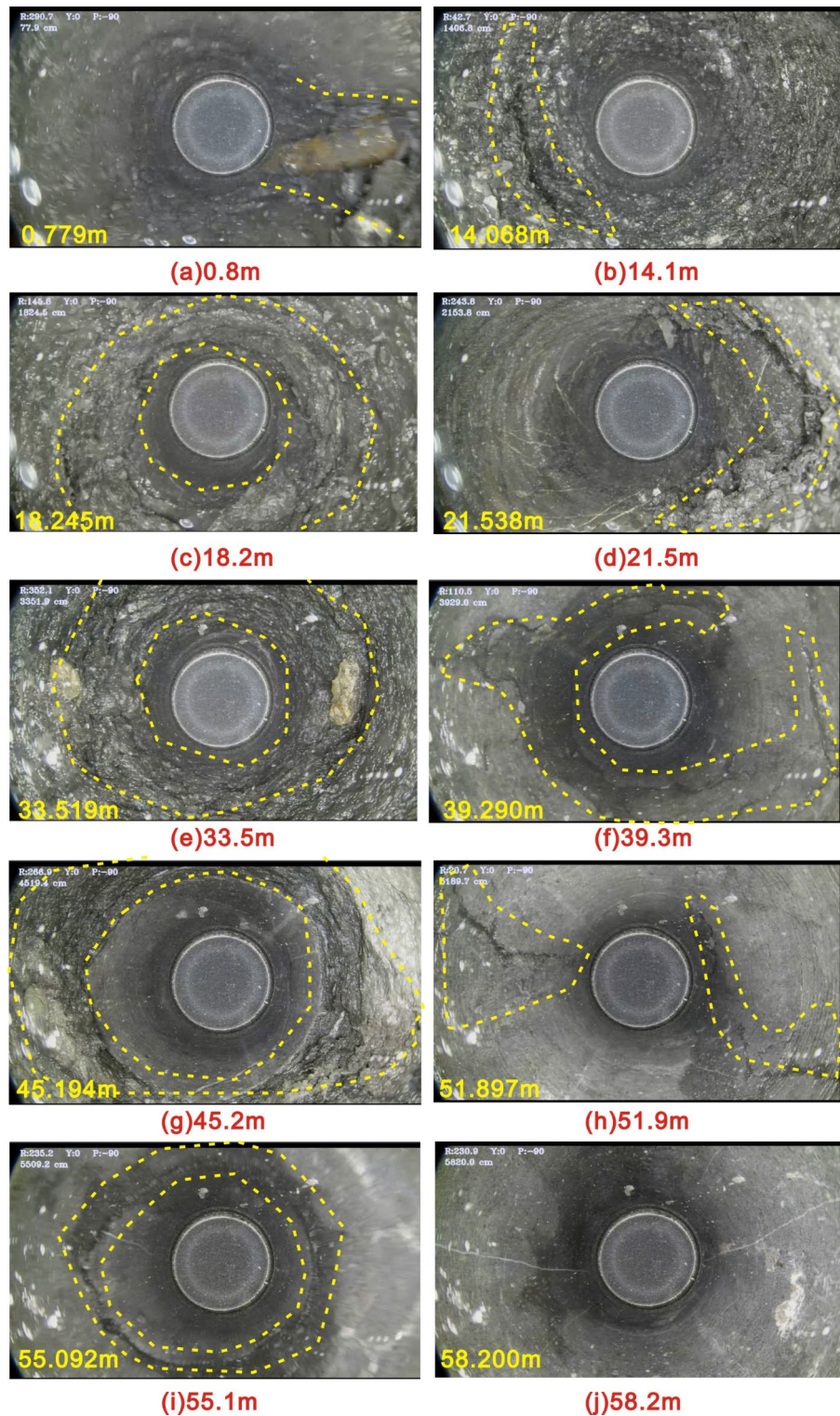


Fig. 13. Borehole imaging results.

working face. Subsidence of the overburden rock also gradually increases, with the displacement curve taking on an “arch” shape. The vertical stress peak and stability of the key stratum of the roof increases with increasing working face advancing distance.

(4) The process of water-conducting fracturing of the mining roof rock can be divided into three stages: (1) slow growth; (2) rapid growth; (3) stable growth. The key stratum of the overburden rock has a significant influence on the development of water-conducting fractures, with a maximum development height of the water-conducting fracture zone of 46.12 m. The actual development height of the water-conducting fracture zone is

42–51.8 m. The results of this study confirm that the plastic zone method is reliable for the analysis of evolution of water-conducting fractures, and are of great significance for guiding practical engineering.

Data availability

All data, models, and code generated or used in the course of the research appear in the submitted article. As some of the data in this article will be used in the research team's next research program, the datasets generated and/or analyzed in this study are not publicly available but can be obtained from the corresponding authors upon reasonable request.

Received: 19 August 2024; Accepted: 13 January 2025

Published online: 20 January 2025

References

- Wang, D., Tian, C., Mao, J. & Chen, F. Forecasting coal demand in key coal consuming industries based on the data-characteristic-driven decomposition ensemble model. *Energy* **282**, 128841 (2023).
- Wang, D., Sui, W. & Ranville, J. F. Hazard identification and risk assessment of groundwater inrush from a coal mine: a review. *Bull. Eng. Geol. Environ.* **81**, 421 (2022).
- Sakhno, I., Sakhno, S., Petrenko, A., Barkova, O. & Kobylanskyi, B. Numerical simulation of the surface subsidence evolution caused by the flooding of the longwall goaf during excavation of thin coal seams. *IOP Conf. Ser. Earth Environ. Sci.* **1254**, 012057 (2023).
- Jiao, L., Yang, R., Chen, B., Zhang, Y. & Variation Determinants and prediction of carbon emissions in Guizhou, a new economic growth Pole in southwest China. *J. Clean. Prod.* **417**, 138049 (2023).
- Zhang, T. et al. Spatial patterns and controlling factors of the evolution process of karst depressions in Guizhou province, China. *J. Geogr. Sci.* **33**, 2052–2076 (2023).
- Gao, Z., Xu, G., Li, H., Su, D. & Liu, Y. Bed Separation Formation Mechanism and Water Inrush Evaluation in Coal Seam Mining under a Karst Cave Landform. *Processes* **11**, 3413 (2023).
- Zhu, H. et al. Study of the Dynamic Development Law of Overburden Breakage on Mining faces. *Sci. Rep.* **10**, 6555 (2020).
- Zhang, P. D. et al. Study on overburden failure characteristics and displacement rule under the influence of deep faults. *Front. Earth Sci.* **12**, 1388612 (2024).
- Ondra, V. & Titurus, B. Free vibration and stability analysis of a cantilever beam axially loaded by an intermittently attached tendon. *Mech. Syst. Signal. Process.* **158**, 107739 (2021).
- Zhang, J., He, M., Yang, G., Wang, Y. & Hou, S. N00 method with double-sided roof cutting for protecting roadways and Surface Strata. *Rock. Mech. Rock. Eng.* **57**, 1629–1651 (2024).
- Feng, G. et al. Tensile mechanical properties and fracture evolution characteristics of sandstone containing parallel pre-cracks under dynamic loading. *Theor. Appl. Fract. Mech.* **125**, 103849 (2023).
- Alejano, L. R. et al. Block toppling stability in the case of rock blocks with rounded edges. *Eng. Geol.* **234**, 192–203 (2018).
- Zhang, P. et al. Experimental study on the flexural behaviors of ECC-reinforced masonry beams with GFRP mesh. *Eng. Struct.* **315**, 118479 (2024).
- Gomes, T. A., de Resende, T. L. & Cardoso, D. C. T. Shear-transfer mechanisms in reinforced concrete beams with GFRP bars and basalt fibers. *Eng. Struct.* **289**, 116299 (2023).
- Xue, J., Cao, C., Yan, J., Ji, Y. & Chen, J. Coupled DEM-FDM analyses of the effects of falling rock's shape and impact angle on response of granular cushion and rock shed. *J. Rock. Mech. Geotech. Eng.* <https://doi.org/10.1016/j.jrmge.2023.12.028> (2024).
- Zheng, Y. et al. Assessing the Stability of Rock Slopes with respect to Block-Flexure Toppling failure using a force-transfer model and genetic algorithm. *Rock. Mech. Rock. Eng.* **53**, 3433–3445 (2020).
- Li, L., Li, F., Zhang, Y., Yang, D. & Liu, X. Formation mechanism and height calculation of the caved zone and water-conducting fracture zone in solid backfill mining. *Int. J. Coal Sci. Technol.* **7**, 208–215 (2020).
- Cao, J. & Wei, X. Research on mining-induced surface soil cracking mechanism and development depth of downward fracture. *Eng. Fail. Anal.* **160**, 108180 (2024).
- Liu, N. et al. Dynamic characteristics of a ground fissure site. *Eng. Geol.* **248**, 220–229 (2019).
- Chi, M. et al. Simulation analysis of water resource damage feature and development degree of mining-induced fracture at ecologically fragile mining area. *Environ. Earth Sci.* **78**, 88 (2019).
- Wang, H., Song, F., Chen, Y., Li, T. & Ma, G. Stability analysis of fractured rock masses based on an extended key block theory considering the forces between blocks and block rotation. *Tunn. Undergr. Space Technol.* **132**, 104895 (2023).
- Chen, Y. et al. Strength prediction model of fractured dolomite and analysis of mechanical properties based on PFC3D. *Sci. Rep.* **13**, 13368 (2023).
- Zhao, B., He, S., Bai, K., Lu, X. & Wang, W. Elastic wave prospecting of water-conducting fractured zones in coal mining. *Sci. Rep.* **14**, 7036 (2024).
- Wang, Y., Peng, J., Wang, L., Xu, C. & Dai, B. Micro-macro evolution of mechanical behaviors of thermally damaged rock: a state-of-the-art review. *J. Rock. Mech. Geotech. Eng.* **16**, 2833–2853 (2024).
- Guo, L., Hou, K., Sun, H. & Yang, Y. Stability evaluation of the Goaf based on combination weighting and cloud model. *Adv. Civ. Eng.* **2024**, 1–19 (2024).
- Mangal, A. Strata Stability Investigation and Convergence Monitoring (SSICM) in Thick-Seam Depillaring with Caving by Cable Bolting Method. *Min. Metall. Explor.* **38**, 927–944 (2021).
- He, J. et al. A method for predicting the water-flowing fractured zone height based on an improved key stratum theory. *Int. J. Min. Sci. Technol.* **33**, 61–71 (2023).
- Ning, S. et al. Influence of stress distribution in coal seams of non-uniform extremely thick key stratum and disaster-causing mechanisms. *Sci. Rep.* **12**, 14465 (2022).
- Zhang, T. et al. Investigations into Mining-Induced stress–fracture–seepage Field Coupling Effect considering the response of Key Stratum and Composite Aquifer. *Rock. Mech. Rock. Eng.* **52**, 4017–4031 (2019).
- Wang, X., Xie, J., Zhu, W. & Xu, J. The field monitoring experiment of the high-level key stratum movement in coal mining based on collaborative DOFS and MPBX. *Sci. Rep.* **12**, 665 (2022).
- Xu, L. et al. Parameters and surrounding rock control of gob-side driving under double key stratum after roof cutting. *Sci. Rep.* **14**, 5106 (2024).
- Mangal, A. & Paul, P. S. Rock mechanical investigation of strata loading characteristics to assess caving and requirement of support resistance in a mechanized powered support longwall face. *Int. J. Min. Sci. Technol.* **26**, 1081–1087 (2016).
- Jia, H. et al. Numerical simulation and damaged analysis of a simply-supported beam bridge crossing potential active fault. *Eng. Struct.* **301**, 117283 (2024).
- Zhang, N. et al. Study of hydrothermal cycling on deterioration and damage mechanism of sandstone. *J. Porous Media.* **28**, 1–18 (2025).

35. Fan, J. et al. Failure analysis of coal pillars and overburden from underground water reservoir under the mining-water invasion coupling effect. *Eng. Fail. Anal.* **151**, 107406 (2023).
36. Zhou, X. P., Wang, F. H., Qian, Q. H. & Zhang, B. H. Zonal fracturing mechanism in deep crack-weakened rock masses. *Theor. Appl. Fract. Mech.* **50**, 57–65 (2008).
37. Li, Y., Yang, S. Q., Song, Y., Li, K. S. & Wang, Q. H. Three-dimensional numerical simulation on failure mechanical characteristics of fissured sandstone specimens under true triaxial conditions. *Theor. Appl. Fract. Mech.* **131**, 104436 (2024).
38. Gusev, V. N. & Ilyukhin, D. A. Determination of water conducting fracture zone for mining and geological conditions of the verkhnekamsk salt deposit. in *INNOVATION-BASED DEVELOPMENT OF THE MINERAL RESOURCES SECTOR: CHALLENGES AND PROSPECTS* (ed. Litvinenko, V.) 195–204 (CRC Press-Balkema, Leiden, (2019).

Acknowledgements

The authors appreciate the support provided by the funders.

Author contributions

Funding acquisition: L.Z. Methodology: L.Z., X.L., Q.Q. Software: X.L., Q.Q., X.W. Investigation: Y.T., W.R. Writing—original draft: L.Z. Writing—final draft: L.Z., L.X., J.X., X.W. All authors reviewed the manuscript.

Funding

This research was financially supported by the National Natural Science Foundation (52164006), the Guizhou Provincial Science and Technology Plan Project (Qian Ke He Zhi Cheng [2022] General 248), and the Guizhou Provincial Social Funding Projects (LDLFSFW2024-9).

Declarations

Competing interests

We declare that we have no financial or personal relationships with other persons or organizations that could unduly influence our work and that we have no professional or other personal interests of any nature or kind in any product, service, and/or company that could be perceived as influencing the position set out in the manuscript titled Study on The Failure Law of Overlying Strata and The Height of Water Flowing Fractured Zone in Northern Guizhou Coalfield or the review of that manuscript.

Additional information

Correspondence and requests for materials should be addressed to L.Z.

Reprints and permissions information is available at www.nature.com/reprints.

Publisher's note Springer Nature remains neutral with regard to jurisdictional claims in published maps and institutional affiliations.

Open Access This article is licensed under a Creative Commons Attribution-NonCommercial-NoDerivatives 4.0 International License, which permits any non-commercial use, sharing, distribution and reproduction in any medium or format, as long as you give appropriate credit to the original author(s) and the source, provide a link to the Creative Commons licence, and indicate if you modified the licensed material. You do not have permission under this licence to share adapted material derived from this article or parts of it. The images or other third party material in this article are included in the article's Creative Commons licence, unless indicated otherwise in a credit line to the material. If material is not included in the article's Creative Commons licence and your intended use is not permitted by statutory regulation or exceeds the permitted use, you will need to obtain permission directly from the copyright holder. To view a copy of this licence, visit <http://creativecommons.org/licenses/by-nc-nd/4.0/>.

© The Author(s) 2025